Supplementary Information:

Pencil-Paper On-Skin Electronics

Yadong Xu[a,1], Ganggang Zhao[b,1], Liang Zhu[c], Qihui Fei[a], Zhe Zhang[a], Zanyu Chen[b], Fufei An[d], Yangyang Chen[b], Yun Ling[b], Peijun Guo[e], Shinghua Ding[a,f], Guoliang Huang[b], Pai-Yen Chen[c], Qing Cao[d], Zheng Yan[a, b,2]

[a]Department of Biomedical, Biological & Chemical Engineering, University of Missouri, Columbia, Missouri 65211, USA

[b]Department of Mechanical & Aerospace Engineering, University of Missouri, Columbia, Missouri 65211, USA

[c]Department of Electrical and Computer Engineering, University of Illinois at Chicago, Chicago, Illinois, 60607, USA

[d]Department of Materials Science and Engineering, University of Illinois at Urbana-Champaign, Urbana, Illinois 61801, USA

[e]Department of Chemical & Environmental Engineering, Yale University, West Haven, Connecticut 06516, USA

[f]Dalton Cardiovascular Research Center, University of Missouri, Columbia, Missouri 65211, USA

[1]These authors contribute equally to this work.

[2]Corresponding author. E-mail: yanzheng@missouri.edu

www.pnas.org/cgi/doi/10.1073/pnas.2008422117

This PDF file includes:

Methods. Materials, fabrications and characterizations of pencil-paper-based devices.

Materials and regents. Potassium ferricyanide [$K_3Fe(CN)_6$], potassium chloride (KCl), gold chloride trihydrate ($HAuCl_4$), polyaniline, potassium phosphate dibasic (K_2HPO_4), potassium phosphate monobasic (KH_2PO_4), chitosan, uric acid, ascorbic acid, glucose, glucose oxidase, acetic acid, poloxamer 407, and rhodamine B were purchased from Sigma-Aldrich. Iron chloride hexahydrate ($FeCl_3 \cdot 6H_2O$), hydrochloric acid (HCl), sulfuric acid (H_2SO_4), lactic acid (LA) and dimethylformamide (DMF) were purchased from Fisher Scientific. Silbione RT Gel 4717 A/B (Silbione) was received from Elkem Silicones. All chemicals were used as received.

Fabrication of pencil-paper-based biophysical and biochemical sensors. The biophysical sensors were directly drawn on commonly used office-copy papers (DPS; Staples Inc.) using a 9B sketching pencil (Staedtler Mars Lumograph; Pencil Things). Silbione solutions (~70 mg/ml in hexane) were spray-coated onto the non-device covered regions of the paper using a commercial airbrush (G222, Master Airbrush) to improve the stickiness. To fabricate the pencil-paper-based sweat biochemical sensors, graphite electrodes were first drawn onto commonly used office-copy papers using a 9B sketching pencil (The Fine Touch; Hobby Lobby) as the basis electrodes. For the UA sensors, the pencil-drawn graphite working electrodes were treated with CO_2 laser (VLS2.30 universal laser system) to improve electrochemical activities. Here, the setting was fixed at 10% of the maximum power, 6% of the maximum scanning speed, and raster mode. And pristine pencil-drawn graphite electrodes were used as counter electrodes without further treatment. To prepare the pH sensors, around ~50 μL of the polyaniline base solution (20 mg ml^{-1}) was drop-casted onto the pencil-drawn graphite electrodes as the working electrodes. Subsequently, the working electrodes were treated with 1.0 M HCl for 15 min to convert polyaniline base into polyaniline emeraldine salt to improve the electrical conductivity and stability. For the fabrication of the glucose sensors, the pencil-drawn graphite working electrodes were first deposited with AuNPs using $HAuCl_4$ in H_2SO_4 as precursor materials with the chronoamperometry method. Next, Prussian blue was deposited on the AuNPs-decorated pencil-drawn graphite electrodes through the cyclic voltammetry in an aqueous solution including 2.5 mM $K_3Fe(CN)_6$, 2.5 mM $FeCl_3$, 100 mM KCl, and 100 mM HCl. The potential was swept from 0 to 0.5 V (vs. Ag/AgCl) with a scan rate of 20 mV s^{-1}. Finally, the addition of the glucose oxidase and chitosan solution

(20 μl) completed the fabrication process. Here, the solution was prepared by mixing the glucose oxidase solution (10 mg ml^{-1} in 0.1 M phosphate buffer solution, pH 7.2) and chitosan solution (1% chitosan in 2% acetic acid) at a volume ratio of 1:1. Besides, the reference electrodes were prepared by drop-casting Ag/AgCl inks (ALS Co., Ltd) onto the pencil-drawn graphite electrodes, which were dried at 120 ℃ for 5 min. Also, Silbione solutions (~70 mg/ml in hexane) were spray-coated onto the non-device covered regions of the paper to improve the stickiness. To ensure reproducibility and reliability, we used stencil masks, prepared by commercial desktop paper cutting machines, to guide pencil drawing and Silbione coating on flat office papers during the device fabrication, and then attached the obtained devices on human bodies for signal recording. The drawing process was repeated for 15 times to achieve desired electrical conductivity.

Fabrication of pencil-paper-based humidity energy harvesters. First, the aforementioned pencil-drawing process using the 9B pencil (The Fine Touch; Hobby Lobby) was used for the fabrication of interdigital electrodes of humidity energy harvesters. The concentration gradient of oxygen-containing groups was generated using the recent reported procedures with minor modifications (RS1). Particularly, a voltage bias of 6 V was applied to the interdigital electrodes using a sourcemeter (2604B, Keithley Instruments Inc.) under a high humidity (90%) environment for 60 s to induce the concentration gradient of oxygen-containing groups. Finally, the capacitive effects were eliminated by a self-discharging process for 30 min, followed by HCl (0.5 M) treatment for 5 min and drying in the air at room temperature.

Design and fabrication of pencil-paper-based dipole antennas. The pencil-paper based dipole antenna is designed and optimized with commercial ANSYS HFSS software. In our simulations, we assume that the sheet resistance of this pencil-drawing graphite is 160 ohm/sq with a thickness of 6 μm. Wave port is applied for the antenna excitation and radiation boundary is employed. Based on the optimized parameters, single-layer dipole antennas were directly drawn on commonly used office-copy papers (DPS; Staples Inc.) using a 9B sketching pencil (Staedtler Mars Lumograph; Pencil Things). The drawing process was repeated for 15 times to achieve desired electrical conductivity (~160 ohm/sq). Afterward, to fabricate multilayer structure, double side tape is utilized to bond each antenna layer together followed by the Sub-Miniature Version A (SMA) connection through silver paste.

Characterizations and measurements. SEM images were taken with a FEI Quanta 600 FEG

Environmental SEM. Raman spectra were collected with a Renishaw Raman microscope. XPS data were recorded on an ESCALAB 250Xi photoelectron spectrometer (Thermo Fisher Scientific) with Al Kα (1486.6 eV). EDS data were taken by iXRF EDS Elemental Analysis System. Mechanical properties were measured with a dynamic tensile tester (Mark-10). Skin adhesion was measured with a force gauge (M5-05). The open-circuit voltage and short-circuit current of the energy harvester were measured by a digital sourcemeter (2604B, Keithley Instruments Inc.). Water vapor transmission rate was evaluated based on ASTM96 at 35 °C. On-skin temperature sensors were calibrated using thermocouples (SA1-K, OMEGA Engineering) with a thermometer (HH309A, OMEGA Engineering). Infrared images were captured with a commercial thermal camera (FLIR E6). Humidity was recorded using a traceable hygrometer (Fisher Scientific). The antennas' reflection coefficient (S_{11}) measurements were conducted using Vector Network Analyzer (VNA) with the pre-calibrated range from 1 to 6 GHz. The radiation pattern was measured in the anechoic chamber room with our under-test antenna acting as transmitter (T_x), which transmits a fixed 20 dBm radio wave generated by signal generator. A broadband horn antenna with 16.5 dBi realized gain at 2.6 GHz is used as receiver (R_x) and the data is recorded by spectrum analyzer. Finally, the radiation pattern can be calculated based on the Friis equation.

Electrophysiological signals were recorded with PowerLab T26 (AD Instruments). The resistances and impedances were measured with LCR Meter (IM3523, HIOKI). Electrochemical characterizations were conducted on an electrochemical station (CHI660E, CH Instruments, Inc.). For on-body measurement of sweat biomarkers, a water-absorbent thin rayon pad was placed between skins and sensors to collect sweat. The pH, UA and glucose in sweat were measured using a pH meter (pH-22, Horiba LAQUAtwin), Uric Acid Assay Kits (QuantiChrom, BioAssay Systems) (RS2), and a Waters Acquity HPLC system coupled to a Bruker Impact II quadrupole time-of-flight mass spectrometer (QTOFMS), respectively. The results were compared to the data obtained with pencil-paper-based sweat biochemical sensors. Continuous recording of UA concentration variations was conducted before and after a purine-rich diet (300 g of canned sardines). Before data collection, pencil-paper enabled UA sensors were calibrated using the DPV method. The forehead of the subject was cleaned with alcohol swabs and then pencil-paper sweat sensors were laminated. Data collection was initiated after 5 min of outdoor running. In the research, anisotropic conductive films

(ACF) were used for wiring the on-skin devices to the external data acquisition equipment. The diffusion of dyes into pig skins was imaged with a Nikon FN1 epifluorescence microscope equipped with a CoolSNAP-EZ CCD-camera. The pig skin was procured from local slaughterhouse, which is exempt from approval by the Institutional Animal Care and Use Committee at University of Missouri-Columbia.

Reference

RS1 Yang, C., Huang, Y., Cheng, H., Jiang, L. & Qu, L. Rollable, stretchable, and reconfigurable graphene hygroelectric generators. *Adv. Mater.* **31**, 1805705 (2019).

RS2 Yang, Y. et al. A laser-engraved wearable sensor for sensitive detection of uric acid and tyrosine in sweat. *Nat. Biotechnol.* **38**, 217-224 (2019).

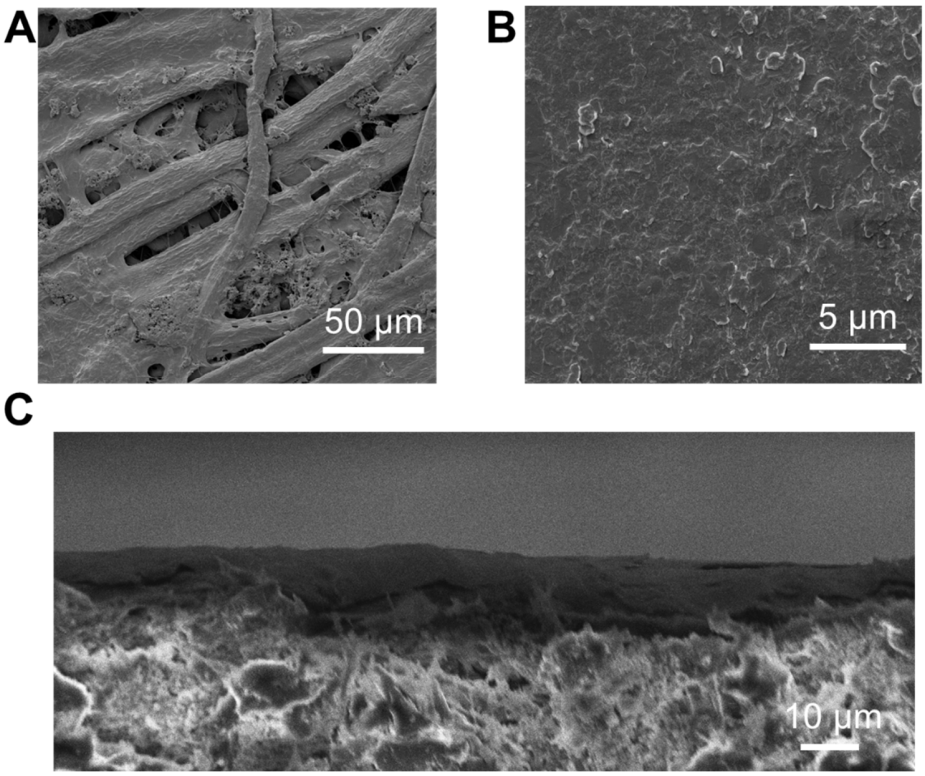

Fig. S1. SEM images of pencil-drawn graphite on office-copy papers. SEM images of the bare regions of the paper (**A**) and pencil-drawn graphite on the paper (**B**). (**C**) Cross-sectional SEM image of pencil-drawn graphite on the paper with 15 writing cycles, indicating the thickness of the graphite layer is around 6 μm.

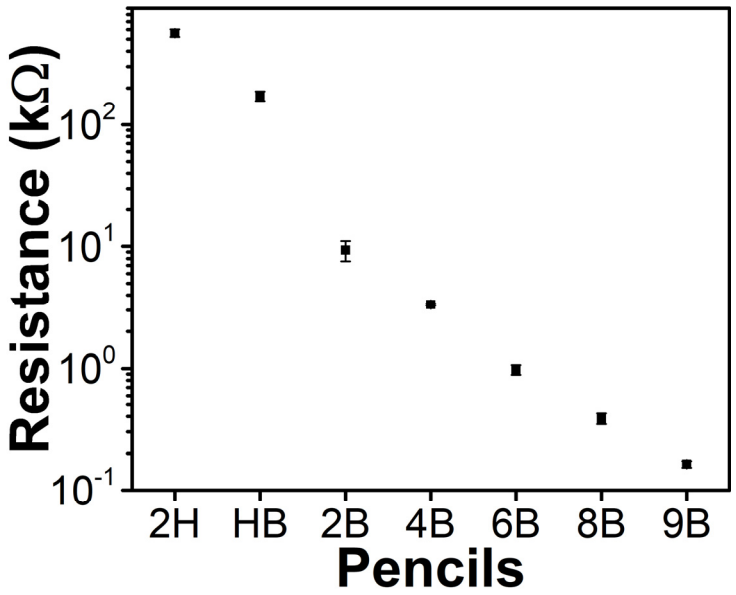

Fig. S2. Sheet resistances of the patterns that were drawn with various types of pencils (15 writing cycles) on office-copy papers. Error bars represent the standard deviations of three individual samples.

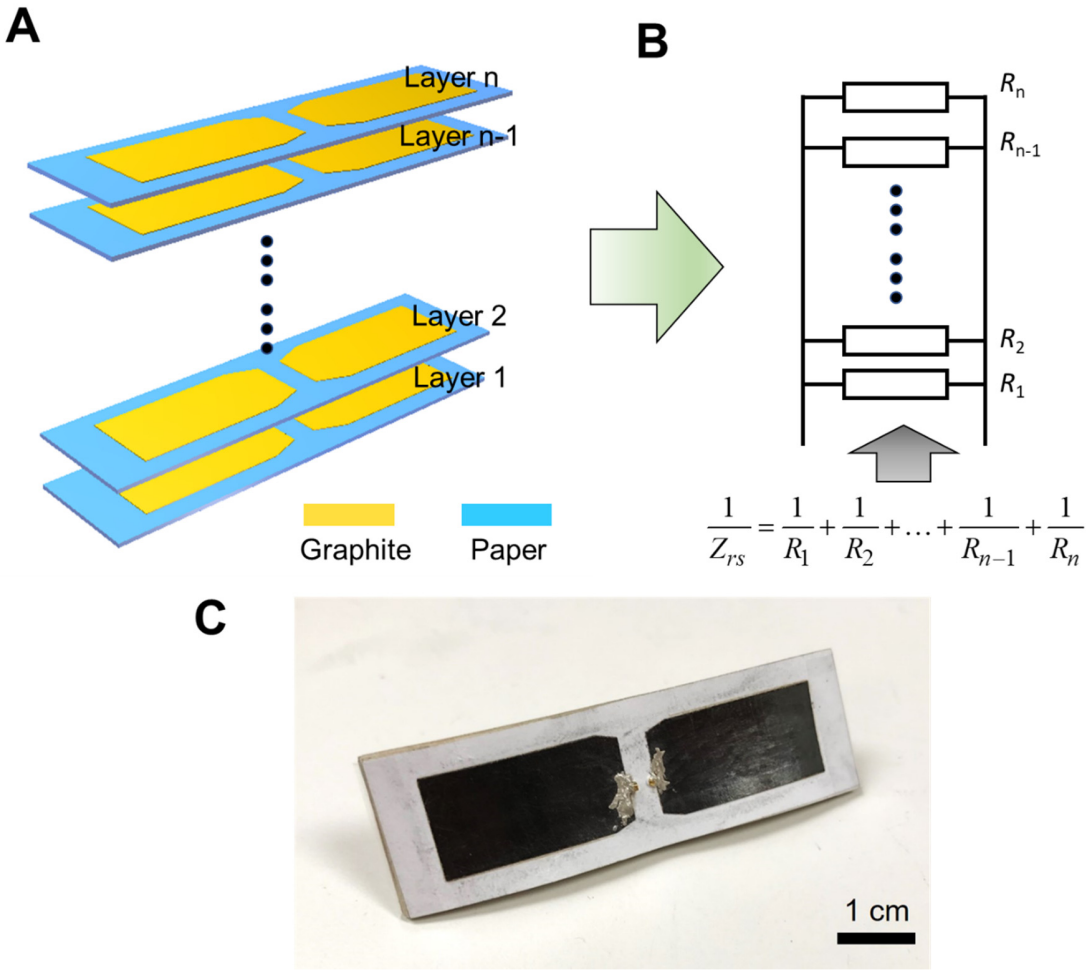

Fig. S3. Pencil-paper-based dipole antennas. Schematic (**A**) and equivalent circuit model (**B**) for the multilayered paper-pencil-based antennas. Each pencil-drawn graphite layers can be seen as a shunt resistance, and the total sheet resistance is reduced by increasing the number of graphite layers. (**C**) Photograph of the fabricated 12 layers of pencil-paper-based dipole antenna.

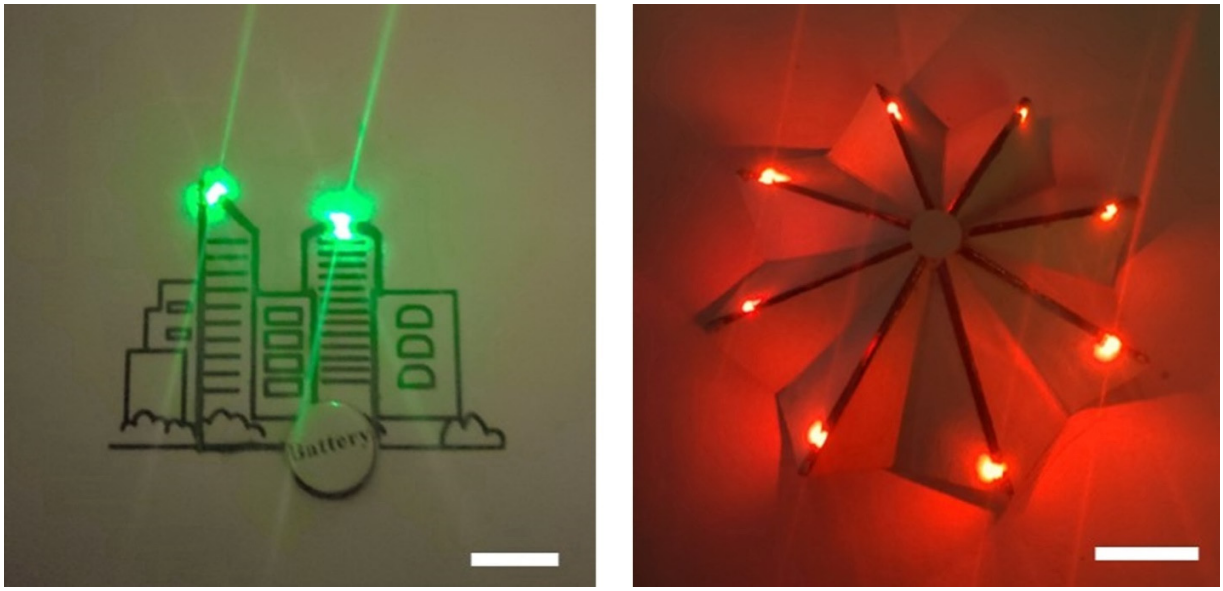

Fig. S4. Pencil-drawn 2D buildings on papers as interconnects integrated with two green LEDs and one battery (left) and origami-inspired umbrella-like 3D paper structures with pencil-drawn interconnects and eight red LEDs (right). Scale bars: 2 cm.

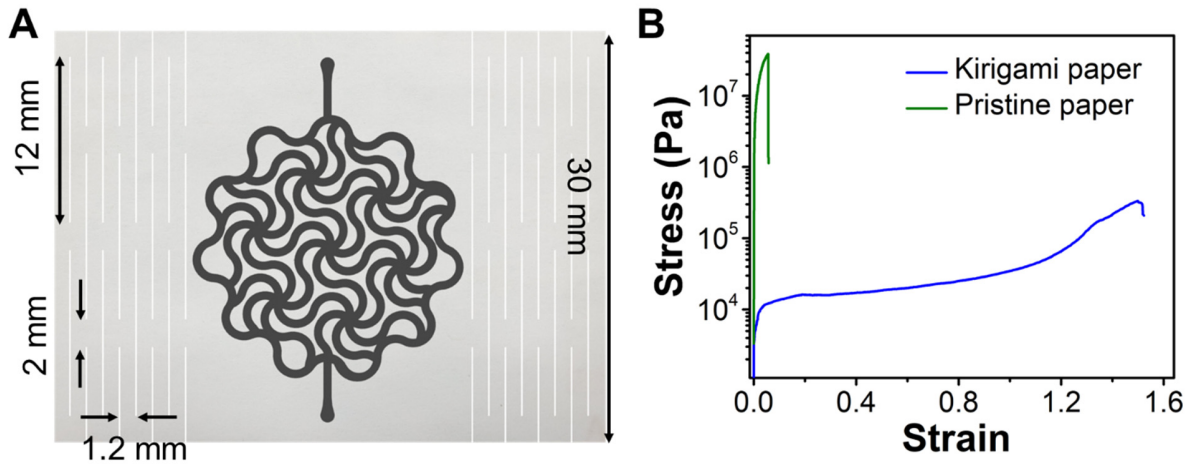

Fig. S5. Highly-stretchable pencil-paper on-skin electronics with kirigami cuts. (A) A schematic illustration of pencil-drawn graphite patterns on papers with kirigami cuts. **(B)** Stress-strain curves of the pristine paper and the paper with kirigami cuts, indicating the significantly improved stretchability and dramatically reduced modulus.

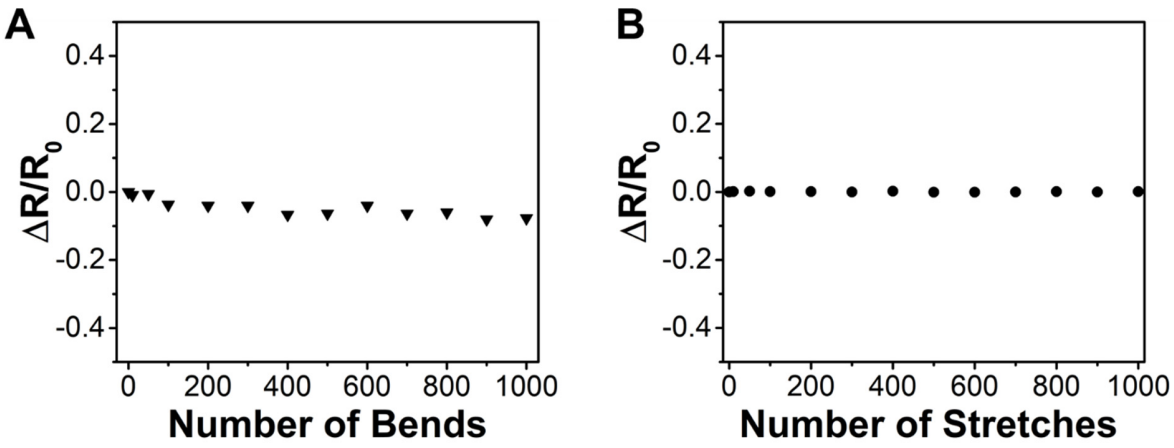

Fig. S6. Normalized electrical resistance changes under cyclic bending and stretching tests. (A) Electrical resistance variations with 1,000 cycles of bending tests under the bending radius of 6 mm. **(B)** Electrical resistance variations with 1,000 cycles of stretching tests under the uniaxial strain of 100%.

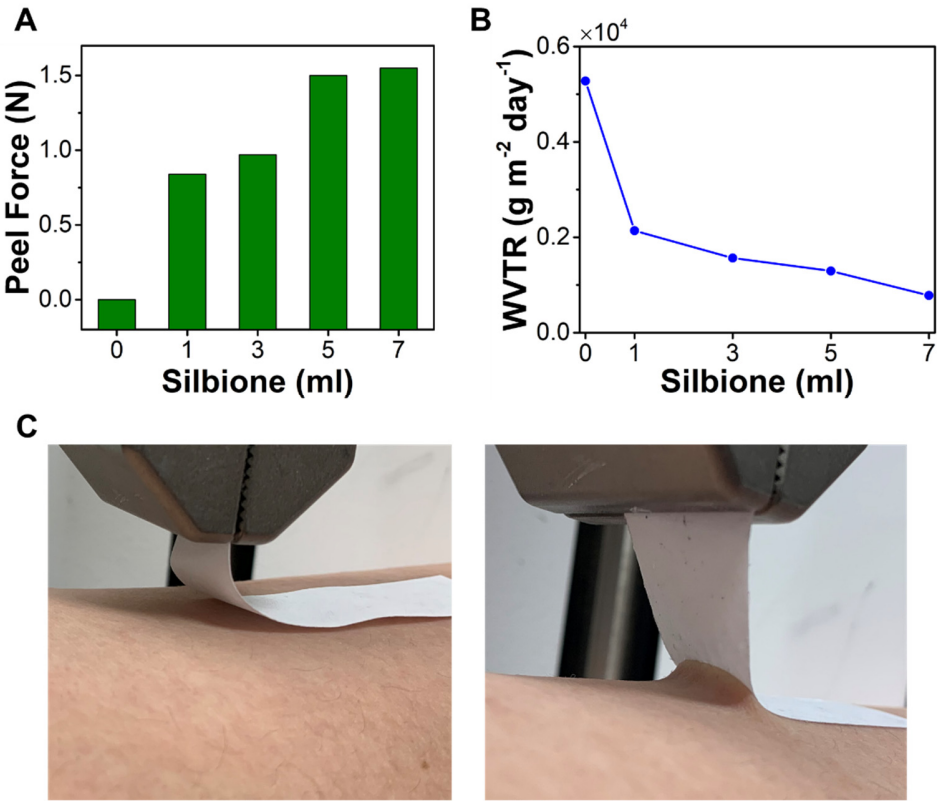

Fig. S7. Optimization of the amount of spray-coated Silbione on paper supporting substrates. Peel-adhesion test (**A**), water vapor transmission rate (WVTR) (**B**) of the papers with different amounts of spray-coated Silbione. **(C)** Optical images of the papers without (left) and with (right) Silbione coating. Here, Silbione solutions were prepared by first equally mixing the base and curing agent, followed by the dilution with hexane to ~70 mg/ml. Then the solution was spray-coated onto the paper substrate at a distance of ~10 cm through a stencil mask using a commercial airbrush (G222, Master Airbrush), and then dried in the air at room temperature. During the peeling test, the sample sizes are 1.5×4 cm^2. After cleaning the skin, alcohol swabs were applied to wet the skin, followed by the lamination of the papers spray-coated with Silbione after the skin was dried. An optimal amount of spray-coated Silbione (the weight ratio of Silbione and paper: ~5:100) was obtained for the fabrication of pencil-paper on-skin electronics based on the trade-off between stickiness and breathability.

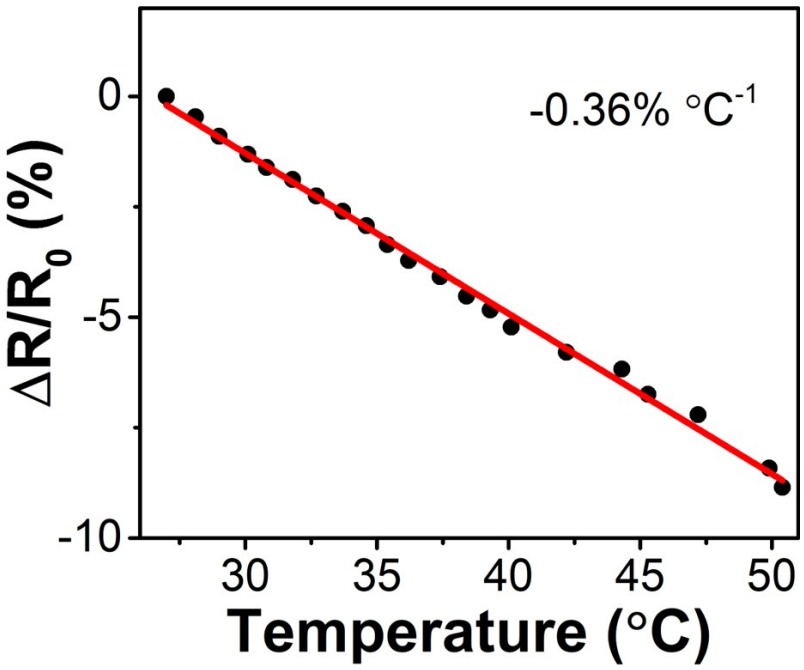

Fig. S8. Calibration plot of the pencil-paper on-skin temperature sensor using a thermocouple in the physiological temperature range.

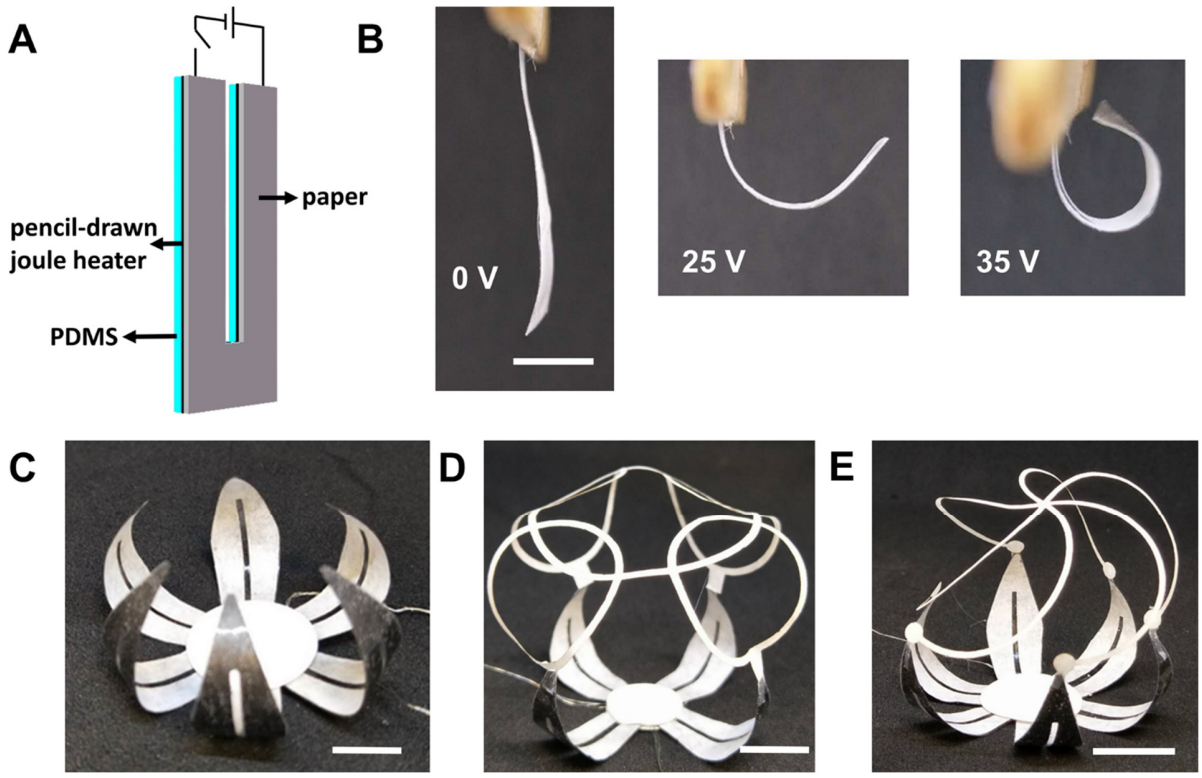

Fig. S9. Pencil-paper-enabled reconfigurable assembly. (A) Schematic illustration of pencil-paper-based electrothermal soft actuators, consisting of paper, pencil-drawn joule heaters and polydimethylsiloxane (PDMS). Upon applying an actuation voltage, joule heaters introduce temperature differences via joule heating. The stress caused by the significant difference in thermal expansion between paper and PDMS can induce bending deformations of actuators toward the paper side (**B**). A variety of 3D structures, such as flow-like structures (**C**) rings-table-like structures (**D**) and cage-like structures (**E**) can be reversibly assembled with pencil-paper-based soft actuators. Scale bars: 1 cm.

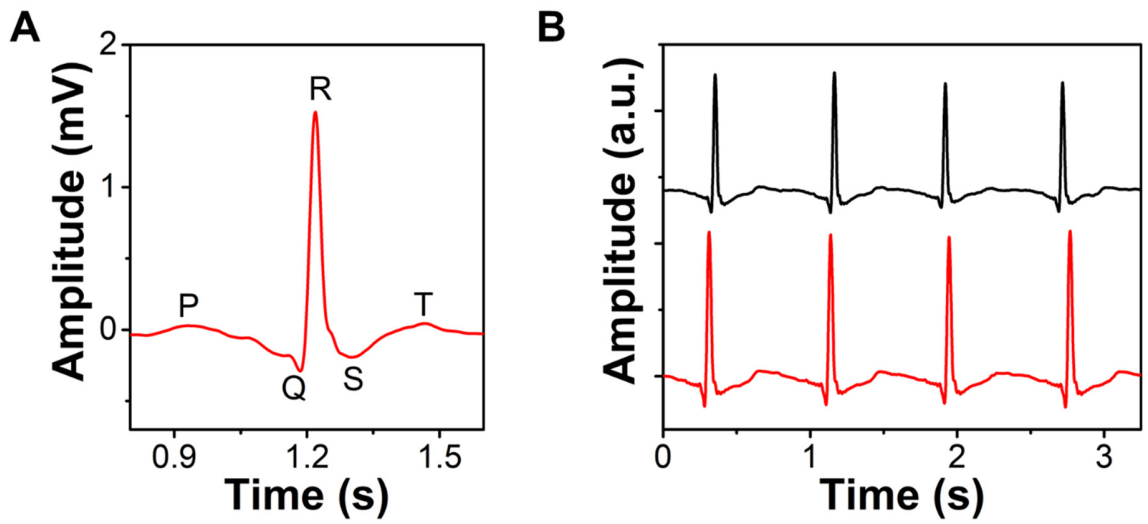

Fig. S10. On-skin ECG measurement. (A) Magnified ECG signals recorded with pencil-paper on-skin electrophysiological sensors, showing distinguishable P-wave, QRS complex and T-wave. **(B)** Comparisons of ECG signals recorded using pencil-paper on-skin electrophysiological sensors (black; SNR: 30 dB) and conventional Ag/AgCl electrodes (red; SNR: 32 dB).

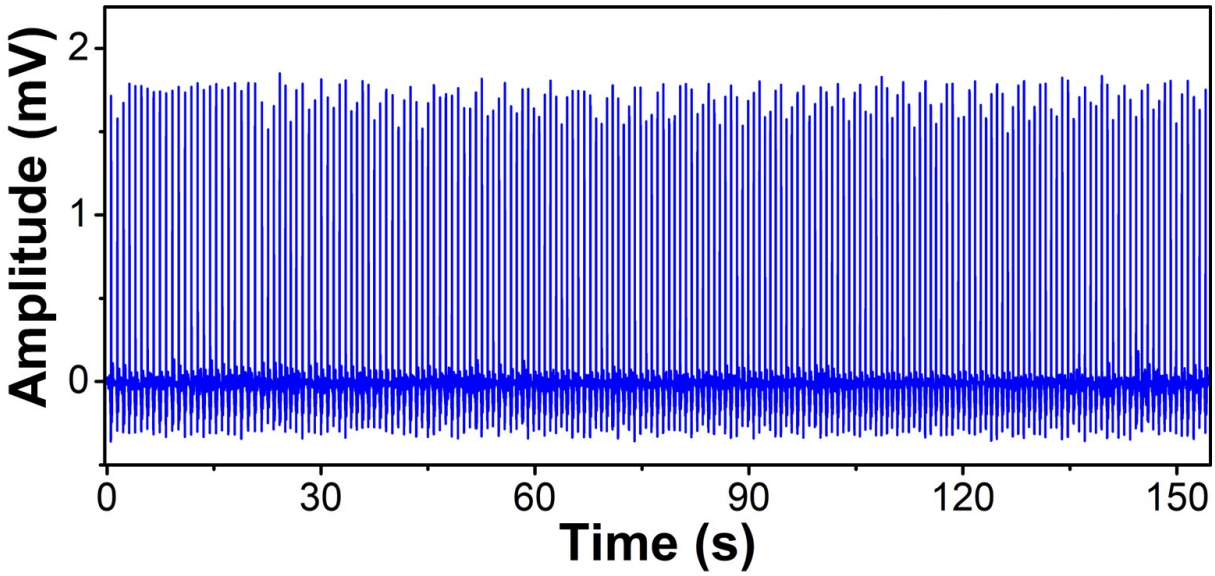

Fig. S11. Continuous recording of ECG signals from the chest of a human volunteer using pencil-paper on-skin electrophysiological sensors, demonstrating high stability.

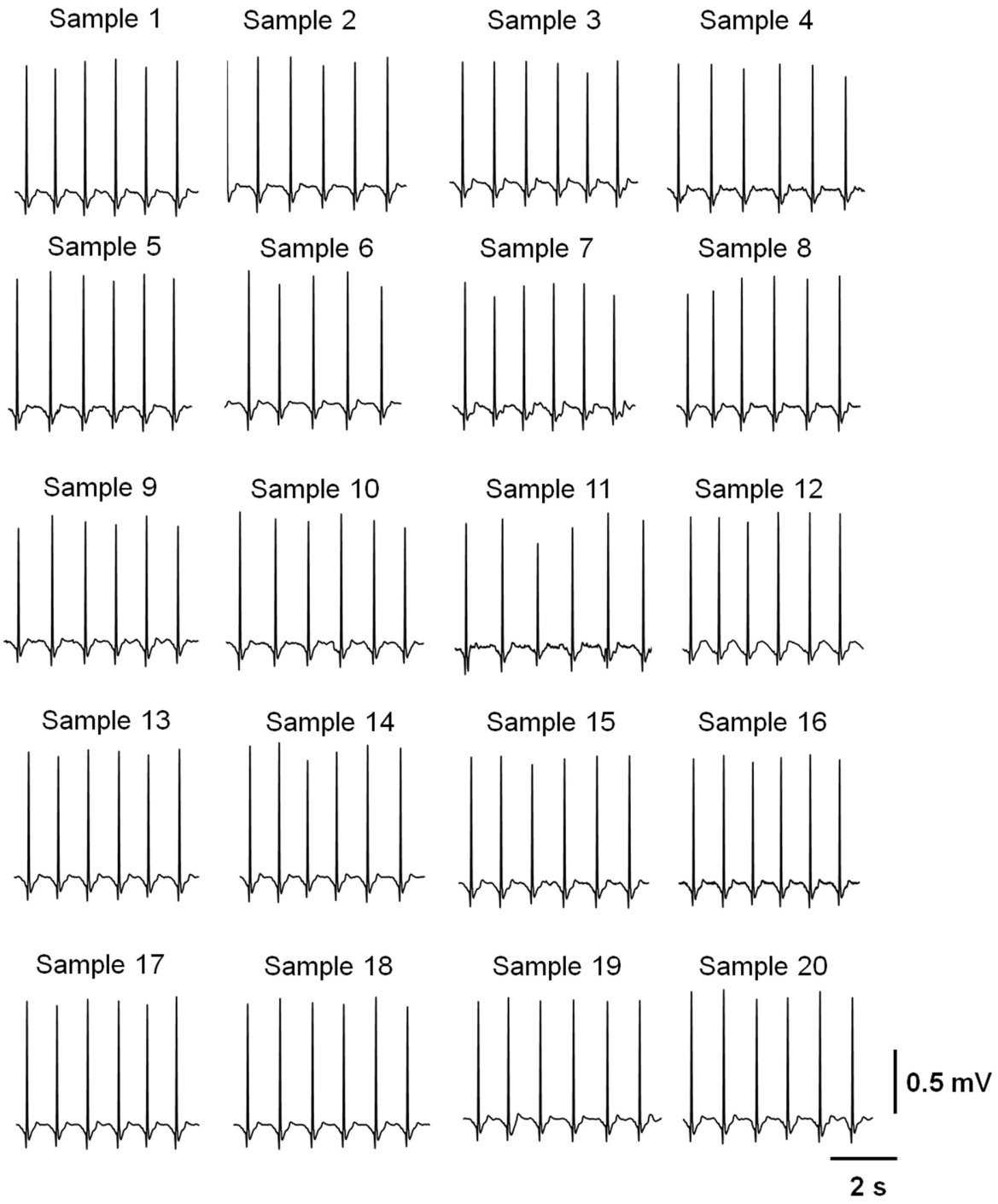

Fig. S12. ECG signals recorded with 20 randomly selected pencil-paper-based on-skin electrophysiological sensors, demonstrating high reproducibility.

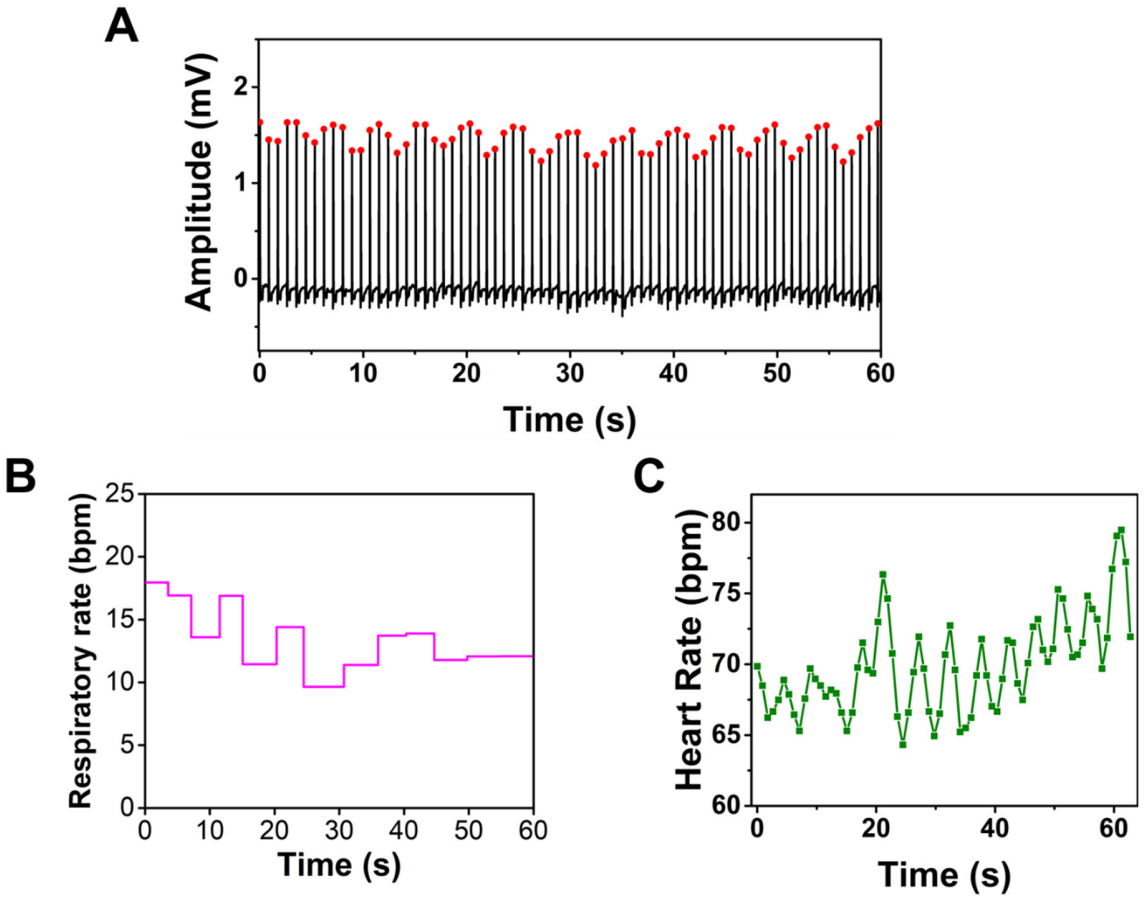

Fig. S13. Analysis of ECG signals recorded with pencil-paper electrophysiological sensors. (A) One-minute continuous ECG recording from the chest of a human volunteer without holding breath. Respiratory rates (**B**) and instantaneous heart rates (**C**) extracted from ECG signals in (**A**).

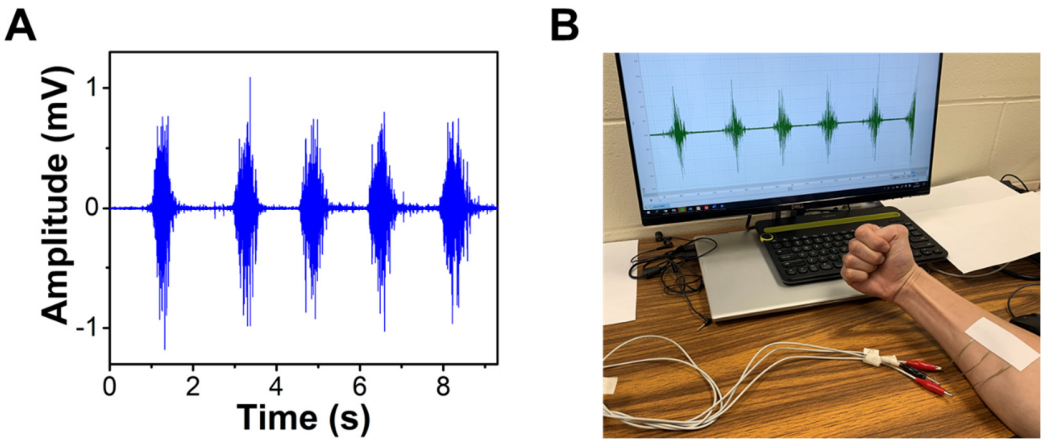

Fig. S14. On-skin EMG recording. (A) EMG recorded from the forearm of a human volunteer using conventional Ag/AgCl gel electrodes. **(B)** A photo of EMG recording with pencil-paper-based sensors.

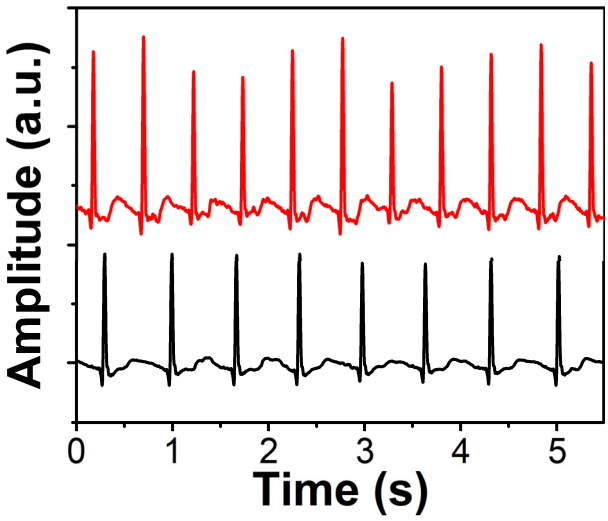

Fig. S15. The ECG signals recorded by the pencil-paper-enabled devices from the chest of a human volunteer before (bottom) and after (top) exercise (running one kilometer) with heavy perspirations, indicating the trivial effects of perspirations on the device performance.

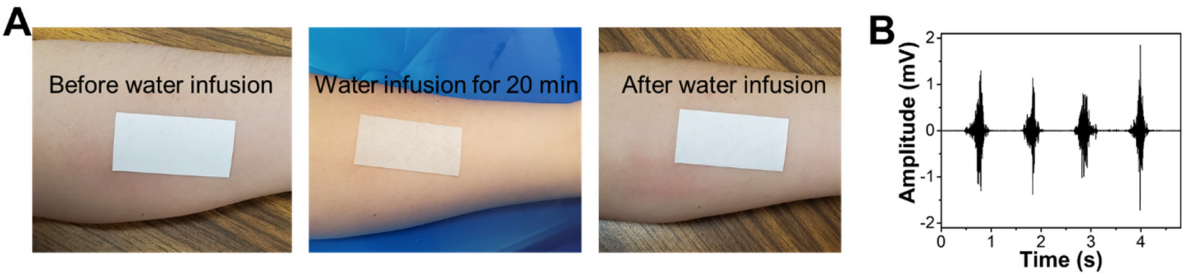

Fig. S16. Stability of pencil-paper-based on-skin electronics with water infusion. (A) Photos of the pencil-paper-based device laminated onto the forearm of a volunteer before, during and after water infusion. **(B)** EMG signals recorded by the device after water infusion. Here, the formation of conformal contact between pencil-paper-based devices and human skins, enabled by Silbione coating, can improve the device stability with water infusion.

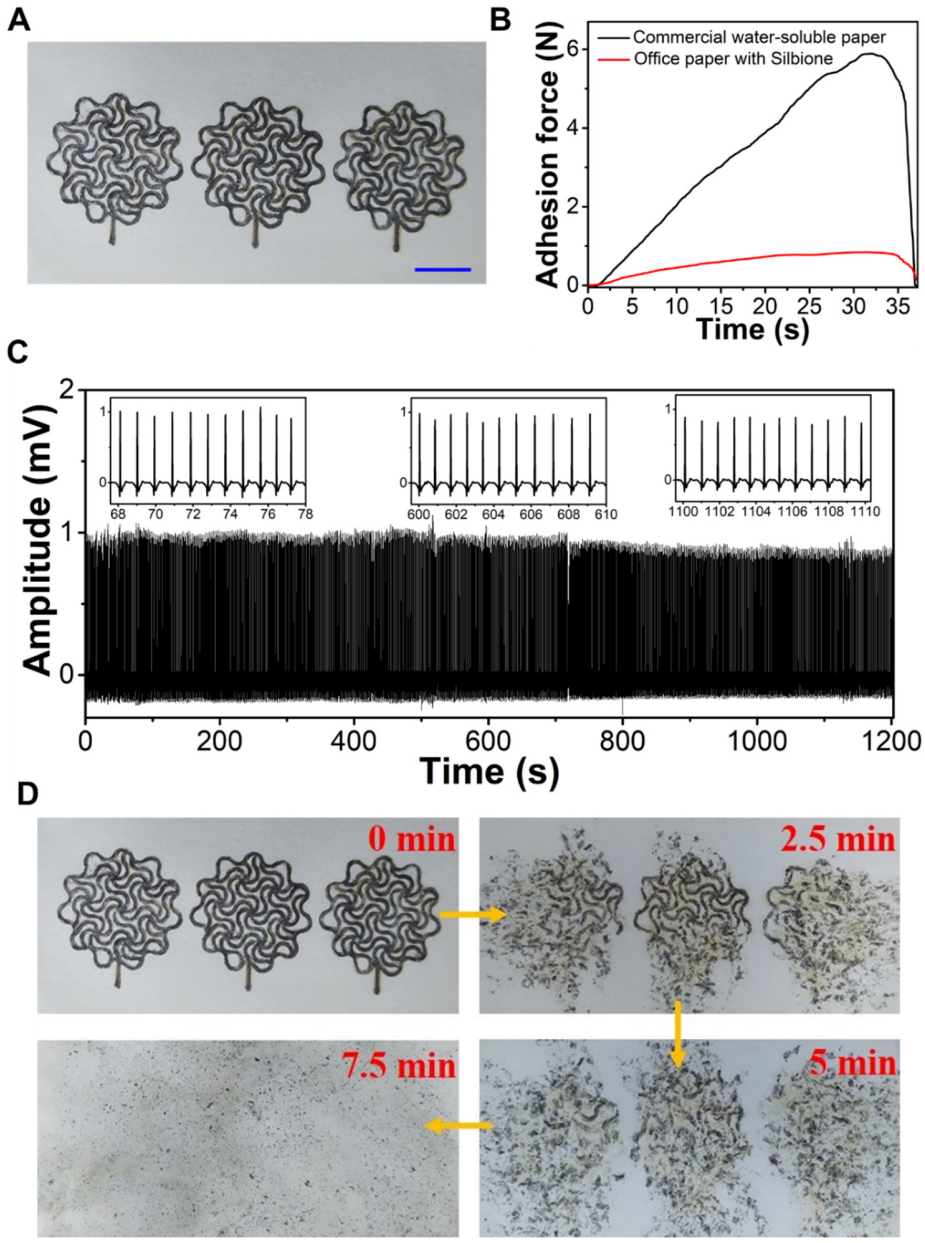

Fig. S17. On-skin bioelectronics based on pencil and adhesive water-soluble paper. (A) A photo of pencil-drawn electrophysiological sensors on adhesive water-soluble papers. Scale bar: 1cm. **(B)** Peel-adhesion tests conducted on the forearm of a human volunteer, indicating adhesive water-soluble paper-based devices is much sticker than office-paper-based devices with Silbione coating. **(C)** Continuous ECG recording for 20 min from a human volunteer, indicating high stability. **(D)** Rapid dissolution of enabled devices in water because of water-soluble paper substrates. Here, non-degradable pencil-drawn graphite only occupies ~3% by weight of the whole device.

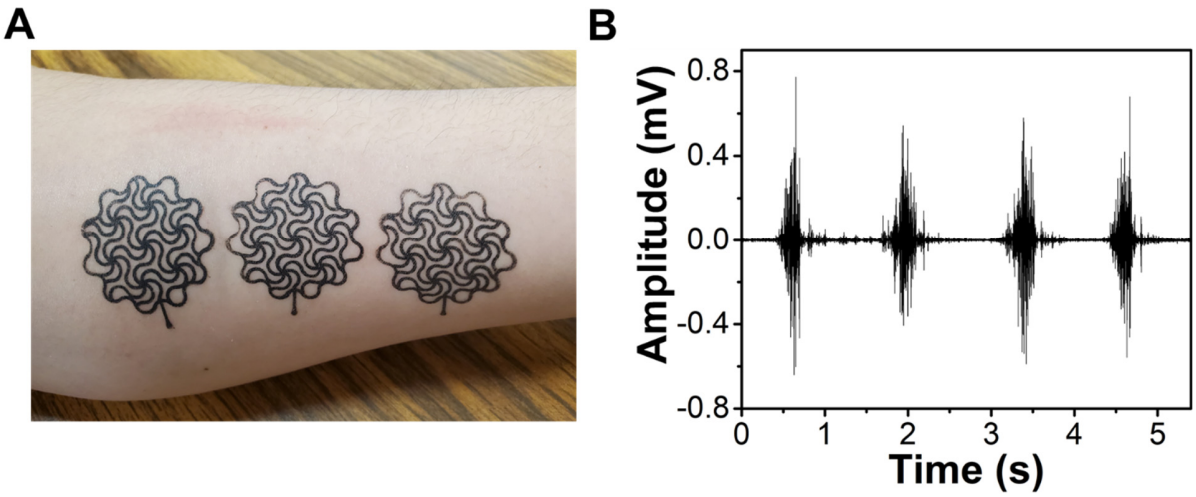

Fig. S18. Optical image of the substrate-free, pencil-drawn electrophysiological sensor on the human forearm (A) and recorded EMG signals by the substrate-free sensor (B).

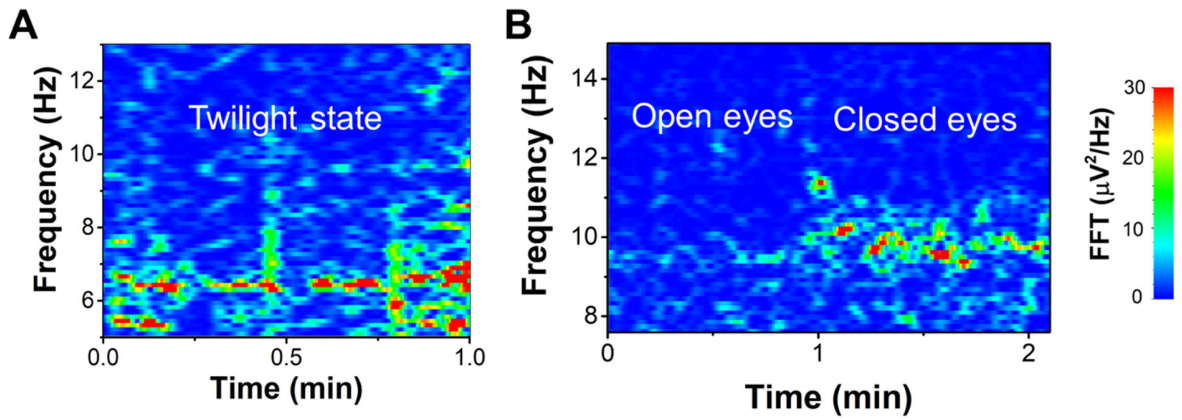

Fig. S19. Time-frequency spectrograms of recorded EEG signals, showing strong theta wave, centered at ~6.5 Hz, at twilight state (A) and intense alpha wave, centered at ~10 Hz, at closed eyes (B).

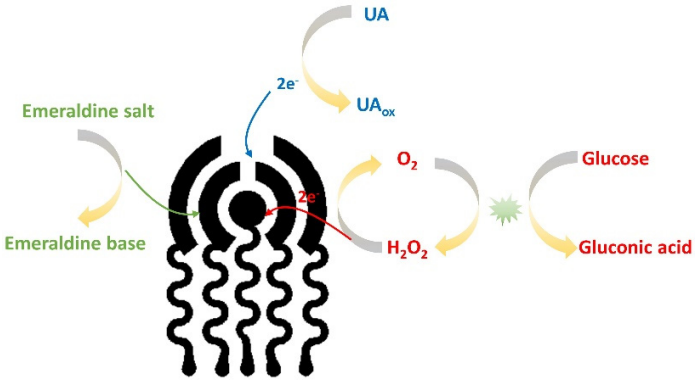

Fig. S20. Schematic illustrations of the working mechanisms of pencil-paper-based pH, uric acid and glucose sensors.

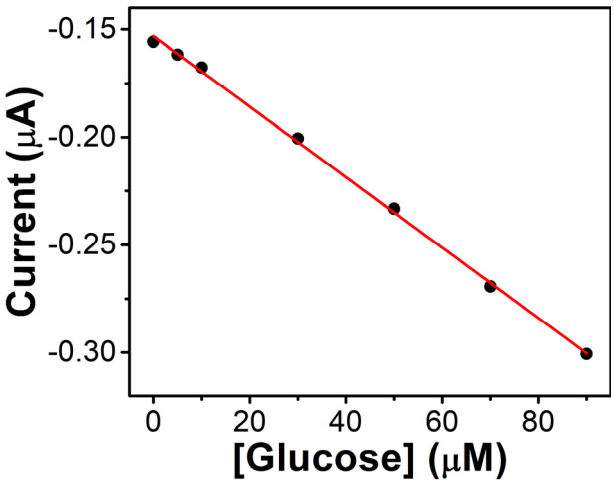

Fig. S21. Calibration plot of the pencil-paper-based glucose sensor in a low glucose concentration range (0-90 μM).

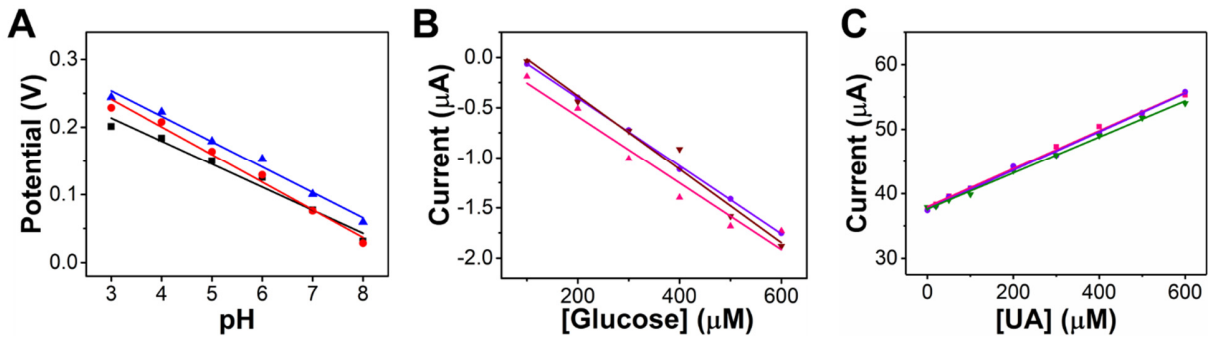

Fig. S22. Reproducibility of pencil-paper-based pH sensors (A), glucose sensors (B) and UA sensors (C). The sensitivities of pH, glucose and UA sensors are 34.4±0.42 mV/decade, 3.46±0.181 nA μM^{-1}, 28.6±1.89 nA μM^{-1}, respectively.

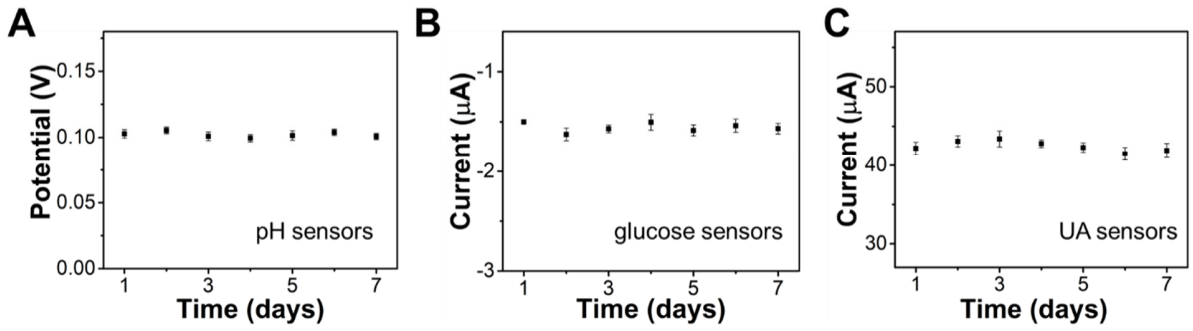

Fig. S23. Long-term stability of pencil-paper-based pH sensors (A), glucose sensors (B) and UA sensors (C).

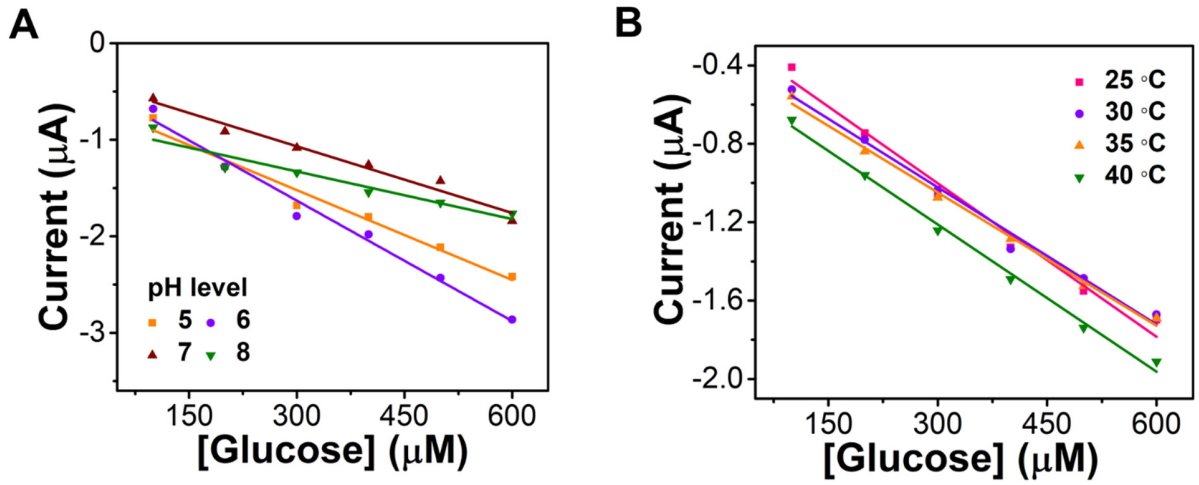

Fig. S24. The dependence of sweat glucose measurement on pH (A) and temperature (B).

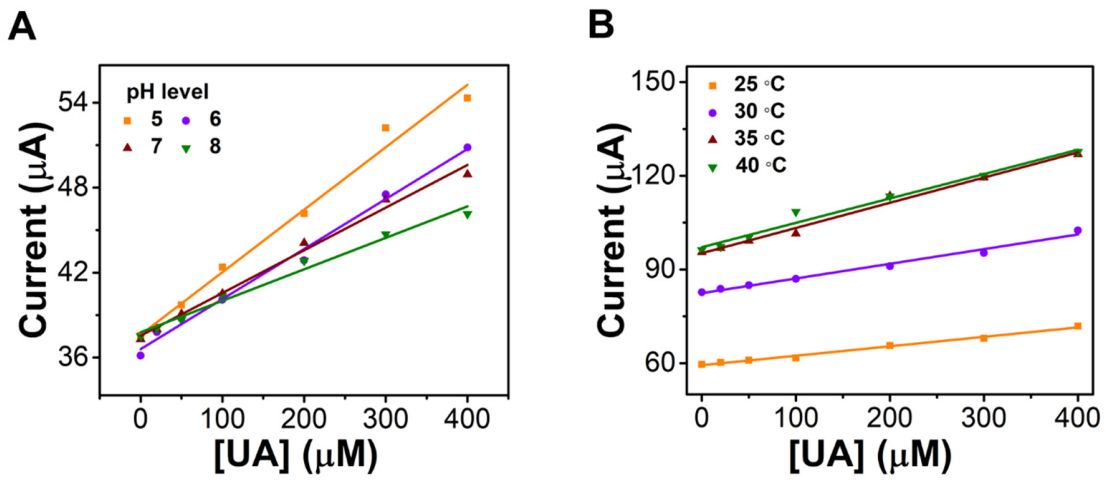

Fig. S25. The dependence of sweat UA measurement on pH (A) and temperature (B).

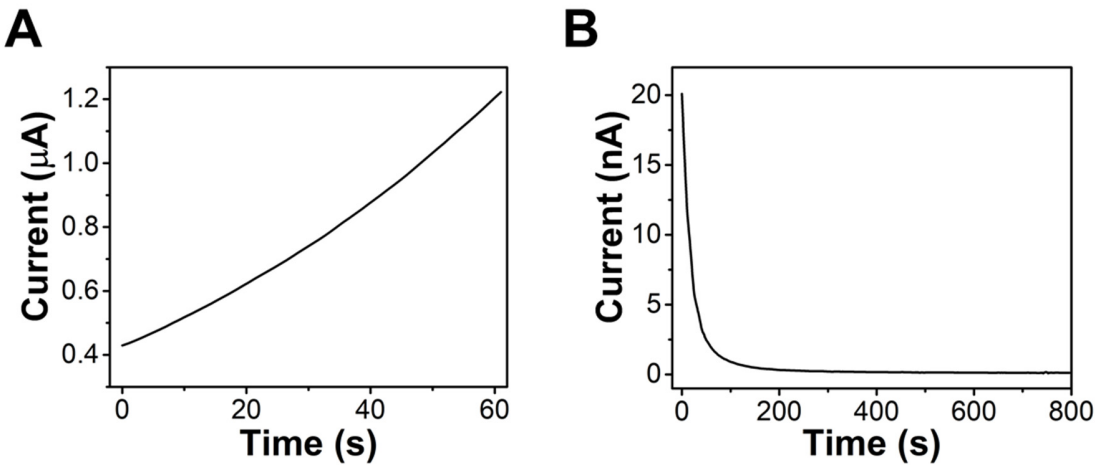

Fig. S26. Current-time profiles of the moisture-electric polarization process of the cellulose paper between two pencil-drawn graphite electrodes. (A) Current plot during the polarization process with an applied voltage of 6 V at a relative humidity of ~90% for 60 s. **(B)** Current plot during the discharging process to eliminate the capacitance effect due to the polarization.

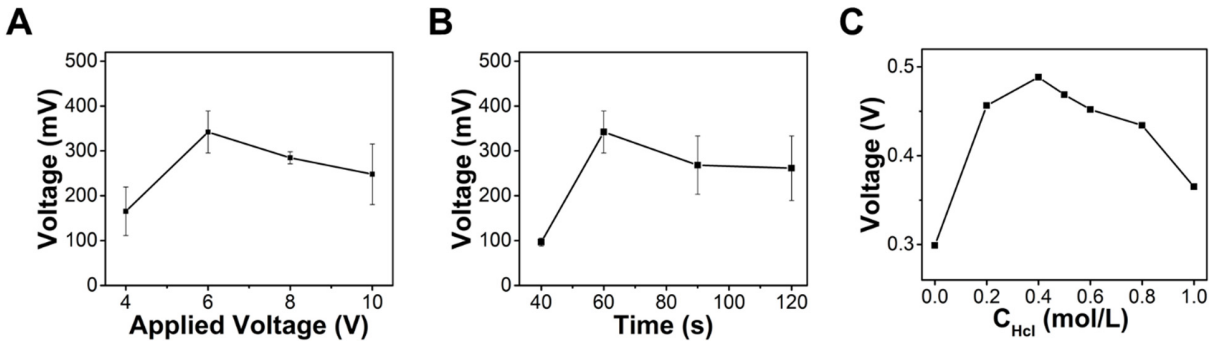

Fig. S27. Optimization of fabrication parameters of pencil-paper-based humidity energy harvesters. **(A-B)** Output voltages of the energy harvesters when exposed to a relative humidity of ~ 95%, which were made using different applied polarization voltages for 60 s (**A**) or with a fixed polarization voltage of 6 V for different polarization times (**B**). Here, the relative humidity for the moisture-electric polarization process is ~90%. **(C)** Output voltages of energy harvesters when exposed to a relative humidity of ~ 95%, which were treated using HCl with different concentrations for 5 min. Here, the polarization process was conducted with an applied voltage of 6 V for 60 s at a relative humidity of ~90%.

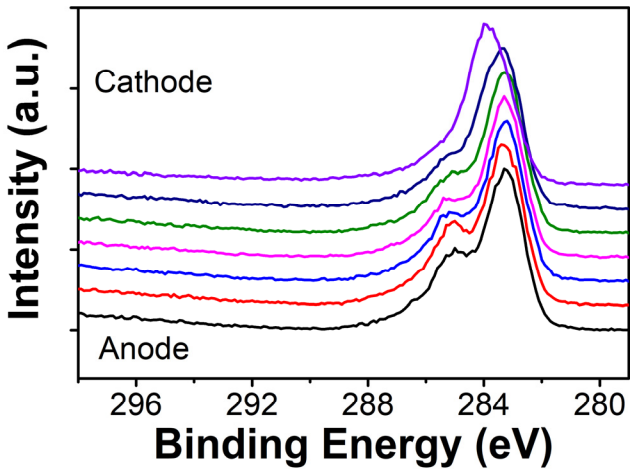

Fig. S28. XPS spectra of polarized cellulose papers at different locations between two pencil-drawn graphite electrodes, indicating an increased concentration of oxygen-containing groups from the cathode to the anode.

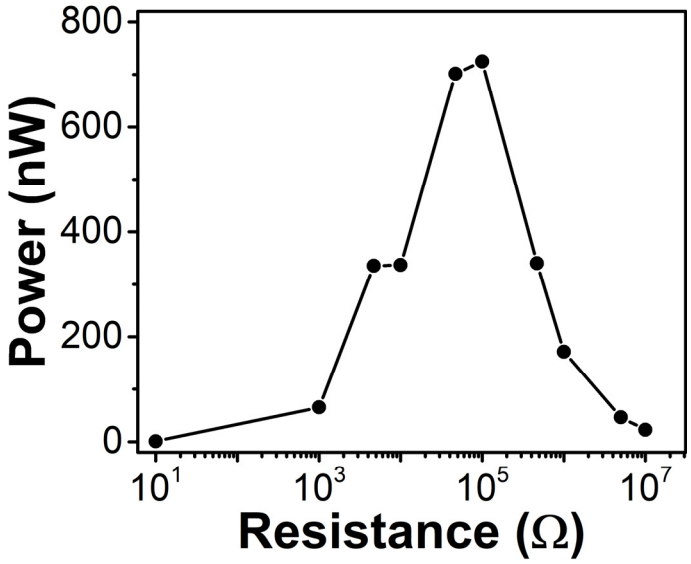

Fig. S29. Generated peak powers of pencil-paper-based humidity energy harvesters, which are connected to the external load resistors with different resistances.

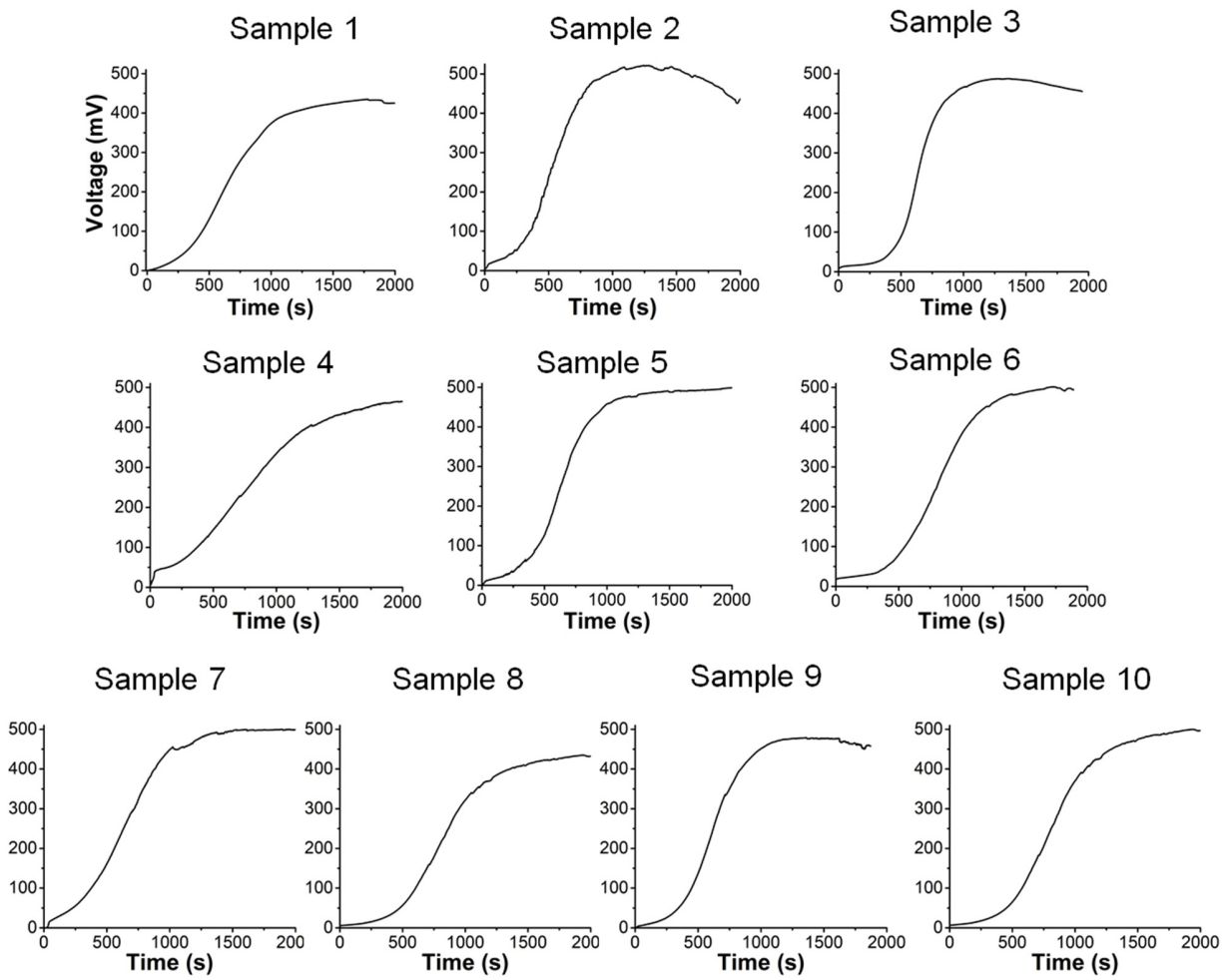

Fig. S30. Dynamic responses of output voltages of 10 randomly selected pencil-paper-based humidity energy harvesters when exposed to a relative humidity of ~95%, demonstrating high reproducibility.